Rank-adaptive dynamical low-rank integrators for first-order and second-order matrix differential equations

Marlis Hochbruck, Markus Neher, Stefan Schrammer

CRC Preprint 2022/13, February 2022

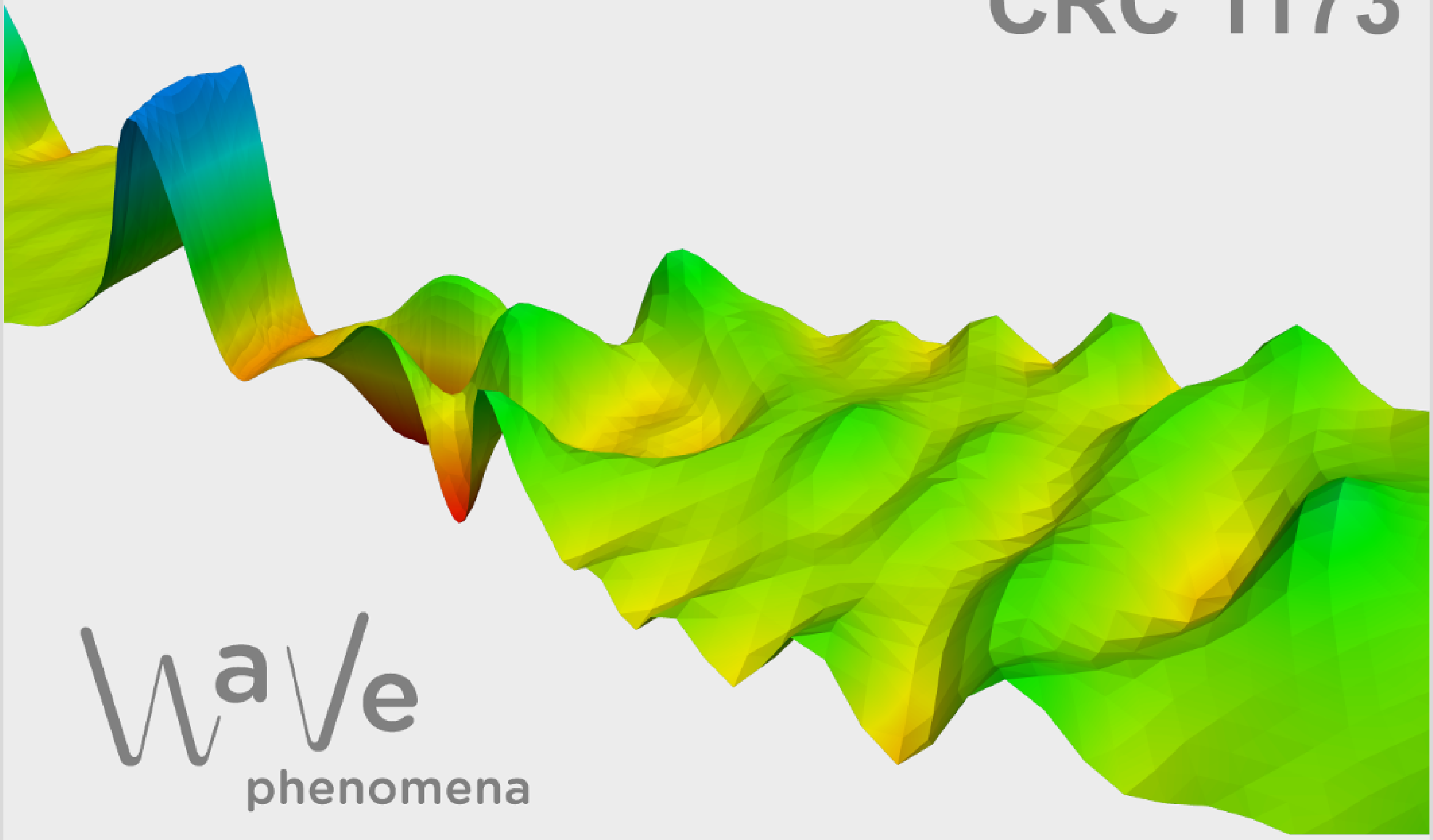

Participating universities

Universität Stuttgart

EBERHARD KARLS UNIVERSITÄT TÜBINGEN

TU WIEN

Funded by

DFG

ISSN 2365-662X

Rank-adaptive dynamical low-rank integrators for first-order and second-order matrix differential equations

Marlis Hochbruck · **Markus Neher** · **Stefan Schrammer**

Received: date / Accepted: date

Abstract Dynamical low-rank integrators for first-order problems have been studied extensively since the 2010s. Recently, dynamical low-rank integrators for second-order problems have been developed in [10]. In this paper, we propose a novel strategy for choosing the rank adaptively, which is applicable for integrators of first and second-order equations. Our adaptive algorithms are based on a combination of error estimators for the local time-discretization error and for the low-rank error. Numerical experiments illustrate the performance of the new integrators.

Keywords dynamical low-rank approximation, matrix differential equations, rank-adaptivity

Mathematics Subject Classification (2010) 65L04, 65L05

1 Introduction

Dynamical low-rank integrators [15,17] have been designed for the approximation of large, time-dependent matrices which are solutions to first-order matrix differential equations

$$A'(t) = F\big(A(t)\big), \quad t \in [0,T], \qquad A(0) = A_0 \in \mathbb{C}^{m\times n}, \tag{1}$$

whose solutions can be well approximated by low-rank matrices. The projector-splitting integrator introduced in [17] has particularly favorable properties. Is is robust in the presence of small singular values, which appear in the case of over-approximation, i.e., when the approximation rank is chosen larger than the rank of the solution $A(t)$ of (1). A variant of this method adapted to strongly dissipative problems was presented in [5]. Another variant tailored for stiff first-order matrix differential equations was introduced in [20].

Marlis Hochbruck · Markus Neher · Stefan Schrammer
Institute for Applied and Numerical Mathematics, Karlsruhe Institute of Technology, Germany,
E-mail: marlis.hochbruck@kit.edu, markus.neher@kit.edu, stefan.schrammer@kit.edu

Recently, a novel dynamical low-rank integrator for second-order matrix differential equations

$$A''(t) = F\big(A(t)\big), \quad t \in [0,T], \qquad A(0) = A_0, \quad A'(0) = B_0, \tag{2}$$

was constructed in [10]. Is is based on a Strang splitting of the equivalent first-order formulation and the projector-splitting integrator [17]. This integrator is also robust in the case of over-approximation and shows second-order convergence in time. Furthermore, with a few modifications, it is suited for stiff second-order matrix differential equations.

In applications, rank-adaptivity turns out to be essential for the efficiency of the algorithm. For first-order equations, in [4] a rank-adaptive variant of the unconventional integrator [5] was proposed. However, since its construction is tailored to this particular method, it cannot be applied to the projector-splitting integrator [17]. In [6], rank-adaptivity for tensor methods for high-dimensional PDEs was based on a functional tensor train series expansion. For the special case of finite-dimensional parametrized Hamiltonian systems modeling non-dissipative phenomena, a rank-adaptive structure-preserving reduced basis method was introduced in [9].

In the present paper, we derive a general strategy for selecting the rank adaptively when using the projector-splitting integrator. Increasing or decreasing the rank from one time step to the next was already proposed in [17] and quite recently in [11]. Our main contribution is a strategy for which the time step of the underlying splitting method, i.e., the Lie-Trotter splitting for first-order and the Strang splitting for second-order problems, is the only input parameter. The goal is to choose the rank such that the error of the dynamical low-rank approximation does not spoil the order of the underlying splitting method applied to the full matrix differential equation. The main idea is to propagate one additional singular value and use it for accepting or rejecting the current time step and for selecting the rank in the next one. The decision is based on an estimator of the global time-discretization error. This adaptivity control is also applicable to the dynamical low-rank integrators for stiff problems. The new dynamical low-rank integrator for (2) uses the projector-splitting integrator in the substeps of the Strang splitting, which allows to control the rank adaptively also for second-order equations, either stiff or nonstiff. Moreover, it can be readily combined with the integrator from [5].

The paper is organized as follows: In Section 2, we briefly recall the projector-splitting integrator introduced in [17] and the ST-LO scheme proposed in [10]. Additionally, we sketch variants of both methods tailored to stiff first-order and second-order differential equations, respectively. Section 3 is devoted to rank-adaptivity. In Section 4, numerical experiments illustrate the performance of the new schemes.

Throughout this paper, m, n, and r are natural numbers, where w.l.o.g. $m \geq n \gg r$. If $n > m$, we consider the equivalent differential equation for the transpose. By $\mathscr{M}_r$ we denote the manifold of complex $m \times n$ matrices with rank r,

$$\mathscr{M}_r = \{\widehat{Y} \in \mathbb{C}^{m\times n} \mid \operatorname{rank}(\widehat{Y}) = r\}.$$

The Stiefel manifold of $m \times r$ unitary matrices is denoted by

$$\mathscr{V}_{m,r} = \{U \in \mathbb{C}^{m\times r} \mid U^H U = I_r\},$$

where I_r is the identity matrix of dimension r and U^H is the conjugate transpose of U.

The singular value decomposition of a matrix $Y \in \mathbb{C}^{m\times n}$ is given by

$$Y = U\Sigma V^H, \quad U \in \mathscr{V}_{m,m}, \quad V \in \mathscr{V}_{n,n}, \quad \Sigma = \operatorname{diag}(\sigma_1,\dots,\sigma_n) \in \mathbb{C}^{m\times n},$$

where $\sigma_1 \geq \ldots \geq \sigma_n \geq 0$ are its singular values. It is well known that for $r < n$, the rank-r best-approximation to Y w.r.t. the Frobenius norm is given by

$$\widehat{Y} = U\widetilde{\Sigma}V^H = \widehat{U}\widehat{\Sigma}\widehat{V}^H,$$

where $\widetilde{\Sigma} = \operatorname{diag}(\sigma_1,\dots,\sigma_r,0,\dots,0)$ and

$$\widehat{U} = U[I_r\ 0] \in \mathscr{V}_{m,r}, \qquad \widehat{V} = V[I_r\ 0] \in \mathscr{V}_{n,r}, \qquad \widehat{\Sigma} = \operatorname{diag}(\sigma_1,\dots,\sigma_r).$$

The Frobenius norm is denoted by $\|\cdot\|$, and the Frobenius inner product by $\langle\cdot,\cdot\rangle$. The symbol $\bullet$ denotes the entrywise or Hadmard product of matrices. For a given step size τ we use the notation $t_k = k\tau$ for any k with $2k \in \mathbb{N}_0$.

2 Dynamical low-rank integrators with fixed rank

In this section we give a review on various low-rank integrators for first and second-order matrix differential equations.

2.1 First-order differential equations

In the dynamical low-rank approximation of the solution to first-order matrix differential equations (1), the approximation $\widehat{A} \approx A$ is determined as solution of the projected differential equation

$$\widehat{A}'(t) = P\big(\widehat{A}(t)\big)F\big(\widehat{A}(t)\big), \quad \widehat{A}(0) = \widehat{A}_0. \tag{3}$$

Here, $P\big(\widehat{A}(t)\big)$ denotes the orthogonal projector onto the tangent space of the low-rank manifold $\mathscr{M}_r$ at $\widehat{A}(t) \in \mathscr{M}_r$. The initial value $\widehat{A}_0$ is typically determined as the rank-r best-approximation to $A(0)$, computed by a truncated SVD. The projector $P\big(\widehat{A}(t)\big)$ is given by

$$P\big(\widehat{A}(t)\big)Z = Z\widehat{V}(t)\widehat{V}(t)^H - \widehat{U}(t)\widehat{U}(t)^H Z\widehat{V}(t)\widehat{V}(t)^H + \widehat{U}(t)\widehat{U}(t)^H Z, \tag{4}$$

cf. [15, Lemma 4.1], where $\widehat{A}(t) \in \mathscr{M}_r$ is decomposed in a non-unique fashion resembling the singular value decomposition into

$$\widehat{A}(t) = \widehat{U}(t)\widehat{S}(t)\widehat{V}(t)^H, \qquad \widehat{U}(t) \in \mathscr{V}_{m,r}, \quad \widehat{V}(t) \in \mathscr{V}_{n,r}, \quad \widehat{S}(t) \in \mathbb{C}^{r\times r} \text{ invertible.} \tag{5}$$

The dynamical low-rank integrator developed in [17], also called the *projector-splitting integrator*, is constructed by performing a Lie-Trotter splitting on the right-hand side of (3) and solving the three subproblems on the low-rank manifold. This approach yields an efficient time-stepping algorithm for computing the desired low-rank approximations. One time-step of the projector-splitting integrator is given in Algorithm 1.

Algorithm 1 Projector-splitting integrator for low-rank approximations to the solution $A(t)$ of (1), single time step, cf. [17, Section 3.2]

```
1: function PRSI($\widehat{U},\widehat{S},\widehat{V},r,\Delta A$)
2:     {input:  factors $\widehat{U},\widehat{S},\widehat{V}$ of rank-$r$ approximation $\widehat{A}=\widehat{U}\widehat{S}\widehat{V}^H \approx A(t)$ with $\widehat{U}\in\mathscr{V}_{m,r}$, $\widehat{V}\in\mathscr{V}_{n,r}$,
3:              $\widehat{S}\in\mathbb{C}^{r\times r}$, functions for matrix-vector multiplication with $\Delta A$ and $\Delta A^H$, where
4:              $\Delta A=\tau F(\widehat{A})$ }
5:
6:     $\widetilde{K}=\Delta A\widehat{V}$
7:     $K=\widehat{U}\widehat{S}+\widetilde{K}$
8:     compute $QR$-decomposition $\widehat{U}\widehat{S}=K$
9:     $\widehat{S}=\widehat{S}-\widehat{U}^H\widetilde{K}$
10:    $L=\widehat{V}\widehat{S}^H+\Delta A^H\widehat{U}$
11:    compute $QR$-decomposition $\widehat{V}\widehat{S}^H=L$
12:
13:    return $\widehat{U},\widehat{S},\widehat{V},L$
14:    {output: factors $\widehat{U},\widehat{S},\widehat{V}$ of rank-$r$ approximation $\widehat{A}=\widehat{U}\widehat{S}\widehat{V}^H\approx A(t+\tau)$ and $L=\widehat{V}\widehat{S}^H$ (optional),
15:             with $\widehat{U}\in\mathscr{V}_{m,r}$, $\widehat{V}\in\mathscr{V}_{n,r}$, $\widehat{S}\in\mathbb{C}^{r\times r}$}
16: end function
```

2.2 Second-order differential equations

For the second-order problem (2), a novel dynamical low-rank integrator named ST-LO scheme (***St**rang splitting combined with the **L**ubich-**O**seledets integrator*) was presented in [10, Section 3]. Given $r_A, r_B \in \mathbb{N}$ and approximations $\widehat{A}_k \approx A(t_k)$ of rank r_A and $\widehat{B}_{k-\frac{1}{2}} \approx A'(t_{k-\frac{1}{2}})$ of rank r_B, it computes approximations $\widehat{A}_{k+1} \in \mathscr{M}_{r_A}$ and $\widehat{B}_{k+\frac{1}{2}} \in \mathscr{M}_{r_B}$ with $\widehat{A}_{k+1} \approx A(t_{k+1})$ and $\widehat{B}_{k+\frac{1}{2}} \approx A'(t_{k+\frac{1}{2}})$, respectively. This integrator is based on the first-order formulation of (2),

$$\begin{bmatrix} A \\ B \end{bmatrix}' = \begin{bmatrix} 0 \\ F(A) \end{bmatrix} + \begin{bmatrix} B \\ 0 \end{bmatrix},$$

combined with a Strang splitting. The subproblems are first-order matrix differential equations,

$$A' = B, \qquad B' = 0, \tag{6a}$$
$$B' = F(A), \qquad A' = 0, \tag{6b}$$

which can be solved exactly. The low-rank matrices $\widehat{A}_{k+1}$ and $\widehat{B}_{k+\frac{1}{2}}$ are obtained by approximating the solutions of (6) by application of Algorithm 1 to

$$\widetilde{B}'_{k-\frac{1}{2}}(\sigma) = F(\widehat{A}_k), \quad \widetilde{B}_{k-\frac{1}{2}}(0) = \widehat{B}_{k-\frac{1}{2}}, \qquad \sigma \in [0,\tau], \tag{7}$$
$$\widetilde{A}'_k(\sigma) = \widetilde{B}_{k+\frac{1}{2}}, \qquad \widetilde{A}_k(0) = \widehat{A}_k, \qquad \sigma \in [0,\tau]. \tag{8}$$

This leads to the dynamical low-rank integrator ST-LO shown in Algorithm 2.

Algorithm 2 DLR integrator for second-order ODEs (2), St-LO scheme, single time step, cf. [10, Algorithm 2]

```
1: function St-LO($\tau, F, \widehat{U}, \widehat{S}, \widehat{V}, \widehat{T}, \widehat{R}, \widehat{W}, r_A, r_B$)
2:     {input: step size $\tau$, right-hand side $F$,
3:             factors $\widehat{U}, \widehat{S}, \widehat{V}$ of rank-$r_A$ approximation $\widehat{A} = \widehat{U}\widehat{S}\widehat{V}^H \approx A(t)$ with $\widehat{U} \in \mathcal{V}_{m,r_A}$, $\widehat{V} \in \mathcal{V}_{n,r_A}$,
4:             $\widehat{S} \in \mathbb{C}^{r_A \times r_A}$,
5:             factors $\widehat{T}, \widehat{R}, \widehat{W}$ of rank-$r_B$ approximation $\widehat{B} = \widehat{T}\widehat{R}\widehat{W}^H \approx A'(t - \frac{\tau}{2})$ with $\widehat{T} \in \mathcal{V}_{m,r_B}$,
6:             $\widehat{W} \in \mathcal{V}_{n,r_B}$, $\widehat{R} \in \mathbb{C}^{r_B \times r_B}$}
7:
8:     $\widehat{B}$-step: $\widehat{T}, \widehat{R}, \widehat{W}, L = $ PRSI$(\widehat{T}, \widehat{R}, \widehat{W}, r_B, \Delta B)$     where $\Delta B = \tau F(\widehat{U}\widehat{S}\widehat{V}^H)$
9:
10:    $\widehat{A}$-step: $\widehat{U}, \widehat{S}, \widehat{V} = $ PRSI$(\widehat{U}, \widehat{S}, \widehat{V}, r_A, \Delta A)$     where $\Delta A = \tau \widehat{T} L^H$
11:
12:    return $\widehat{U}, \widehat{S}, \widehat{V}, \widehat{T}, \widehat{R}, \widehat{W}$
13:    {output: factors $\widehat{U}, \widehat{S}, \widehat{V}$ of rank-$r_A$ approximation $\widehat{A} = \widehat{U}\widehat{S}\widehat{V}^H \approx A(t+\tau)$ with $\widehat{U} \in \mathcal{V}_{m,r_A}$,
14:             $\widehat{V} \in \mathcal{V}_{n,r_A}$, $\widehat{S} \in \mathbb{C}^{r_A \times r_A}$,
15:             factors $\widehat{T}, \widehat{R}, \widehat{W}$ of rank-$r_B$ approximation$\widehat{B} = \widehat{T}\widehat{R}\widehat{W}^H \approx A'(t + \frac{\tau}{2})$ with $\widehat{T} \in \mathcal{V}_{m,r_B}$,
16:             $\widehat{W} \in \mathcal{V}_{n,r_B}$, $\widehat{R} \in \mathbb{C}^{r_B \times r_B}$}
17: end function
```

2.3 Stiff problems

A fixed-rank dynamical low-rank integrator for the stiff first-order problem

$$A'(t) = L_1 A(t) + A(t) L_2 + f\big(A(t)\big), \quad t \in [0,T], \qquad A(0) = A_0, \tag{9}$$

where the norms of $L_1 \in \mathbb{C}^{m \times m}$ and $L_2 \in \mathbb{C}^{n \times n}$ are large and f is a Lipschitz continuous function with moderate Lipschitz constant, was introduced in [20]. It is based on the solution of the subproblems

$$A' = L_1 A + A L_2, \tag{10a}$$
$$A' = f(A). \tag{10b}$$

The solution to (10a) is given by

$$A(t) = \exp(tL_1) A_0 \exp(tL_2). \tag{11}$$

Note that the rank of the initial value is preserved for all times [20, Section 3.2]. In contrast, the rank of the solution of the nonlinear subproblem (10b) may vary in time.

In [20], a low-rank approximation has been computed by applying a Lie-Trotter splitting to (9) and solving the subproblems (10) by the projector-splitting integrator in Algorithm 1. This method is called PRSISTIFF in the following.

For semilinear second-order equations of the form

$$A''(t) = -\Omega_1^2 A(t) - A(t)\Omega_2^2 + f\big(A\big), \quad t \in [0,T], \quad A(0) = A_0, \quad A'(0) = B_0, \tag{12}$$

with Hermitian, positive semidefinite matrices $\Omega_1 \in \mathbb{C}^{m \times m}$ and $\Omega_2 \in \mathbb{C}^{n \times n}$ of large norm and f again Lipschitz continuous, a dynamical low-rank integrator named St-LOstiff was proposed in [10, Section 5]. It is based on the equivalent first-order formulation of the second-order problem (12), where one splits the right-hand side into

$$\begin{bmatrix} A \\ B \end{bmatrix}' = \begin{bmatrix} B \\ -\Omega_1^2 A - A\Omega_2^2 + f(A) \end{bmatrix} = \begin{bmatrix} \omega_1^2 B \\ -\Omega_1^2 A \end{bmatrix} + \begin{bmatrix} \omega_2^2 B \\ -A\Omega_2^2 \end{bmatrix} + \begin{bmatrix} \omega_3^2 B \\ f(A) \end{bmatrix}. \tag{13}$$

The weights $\omega_i \geq 0$, $i = 1,2,3$, can be chosen arbitrarily such that $\omega_1^2 + \omega_2^2 + \omega_3^2 = 1$. A natural choice is $\omega_i^2 = 1/3$. The linear subproblems can be solved exactly. Low-rank approximations to these solutions are obtained by application of the projector-splitting integrator. The nonlinear subproblem is solved approximately with a variant of the ST-LO scheme, cf. [10, Algorithm 3]. Denoting the numerical flows of the linear subproblems by $\phi_\tau^{\Omega_1}$ and $\phi_\tau^{\Omega_2}$, and the numerical flow of the nonlinear subproblem as $\phi_\tau^{\mathscr{S}}$, respectively, one step of the ST-LOSTIFF scheme reads

$$\begin{bmatrix} \widehat{A}_{k+1} \\ \widehat{B}_{k+1} \end{bmatrix} = \left(\phi_{\frac{\tau}{2}}^{\Omega_1} \circ \phi_{\frac{\tau}{2}}^{\Omega_2} \circ \phi_\tau^{\mathscr{S}} \circ \phi_{\frac{\tau}{2}}^{\Omega_2} \circ \phi_{\frac{\tau}{2}}^{\Omega_1} \right) \begin{bmatrix} \widehat{A}_k \\ \widehat{B}_k \end{bmatrix}.$$

3 Rank adaptivity

In many applications, an appropriate rank for computing a low-rank approximation to the exact solution of (2) or (1) is not known a priori and might also vary over time. If the rank is chosen too small, the low-rank approximation lacks accuracy. Conversely, if the rank is chosen too large, the algorithm becomes inefficient.

In the following, we derive rank-adaptive variants of the projector-splitting integrators PRSI and PRSISTIFF for first-order problems and for the ST-LO and the ST-LOSTIFF schemes for second-order problems.

3.1 Selecting the rank

We first discuss the projector-splitting integrator for the first-order problem (1). The idea of our rank-adaptive strategy is to approximate the exact solution of (1) by a low-rank solution of rank r_k in the kth time step, but to propagate a solution of rank $r_k + 1$. The additional information is used as an indicator whether to accept or reject the current time step, and for selecting the rank r_{k+1} for the next time step.

Given $\widehat{A}_k = \widehat{U}_k \widehat{S}_k \widehat{V}_k^H \in \mathscr{M}_{r_k+1}$, a single step of Algorithm 1 yields the approximation $\widehat{A}_{k+1} = \widehat{U}_{k+1} \widehat{S}_{k+1} \widehat{V}_{k+1}^H \in \mathscr{M}_{r_k+1}$. We then compute the singular value decomposition of $\widehat{S}_{k+1}$,

$$\widehat{S}_{k+1} = P_{k+1} \Sigma_{k+1} Q_{k+1}^H, \quad \Sigma_{k+1} = \operatorname{diag}(\widehat{\sigma}_1, \ldots, \widehat{\sigma}_{r_k}, \widehat{\sigma}_{r_k+1}),$$

with $P_{k+1}, Q_{k+1} \in \mathscr{V}_{r_k+1, r_k+1}$, and $\widehat{\sigma}_1 \geq \ldots \geq \widehat{\sigma}_{r_k+1} \geq 0$ so that

$$\widehat{A}_{k+1} = (\widehat{U}_{k+1} P_{k+1}) \Sigma_{k+1} (\widehat{V}_{k+1} Q_{k+1})^H$$

is the singular value decomposition of $\widehat{A}_{k+1}$. Given a tolerance `tol`, we determine r_k such that

$$\widehat{\sigma}_{r_k+1} < \texttt{tol} \leq \widehat{\sigma}_{r_k} \tag{14}$$

by distinguishing three cases:

1. *Augmentation case:* If $\widehat{\sigma}_{r_k+1} \geq \texttt{tol}$, the step is rejected and recalculated with rank $r_k + 2$. Rank augmentation applies to the initial values $\widehat{U}_k, \widehat{S}_k, \widehat{V}_k$ of the current integration step and is performed by adding a zero entry to $\widehat{S}_k$,
$$S^* = \begin{bmatrix} \widehat{S}_k & 0 \\ 0 & 0 \end{bmatrix} \in \mathbb{C}^{(r_k+2)\times(r_k+2)}. \tag{15a}$$
This choice has been motivated by [17, Section 5.2]. The matrices $\widehat{U}_k$ and $\widehat{V}_k$ are augmented by unit vectors $u \in \mathbb{C}^m$ and $v \in \mathbb{C}^n$ such that
$$U^* = \begin{bmatrix} \widehat{U}_k & u \end{bmatrix} \in \mathscr{V}_{m,r_k+2}, \qquad V^* = \begin{bmatrix} \widehat{V}_k & v \end{bmatrix} \in \mathscr{V}_{n,r_k+2}. \tag{15b}$$
Numerical tests indicate that choosing u and v as random vectors and orthonormalizing them against $\widehat{U}_k$ and $\widehat{V}_k$ is reliable and robust, but other choices are also possible. Clearly, $U^*S^*(V^*)^H = \widehat{U}_k\widehat{S}_k\widehat{V}_k^H = \widehat{A}_k$, thus the initial value of the current integration step has not changed. However, the numerical approximation is now able to evolve to rank $r_k + 2$. The step is recomputed with the new initial values U^*, S^*, V^*, and it is again checked if the smallest singular value allows one to accept the step. This procedure is repeated until (14) is satisfied and the step is finally accepted, see Algorithm 3 for details.
2. *Reduction case:* If $\widehat{\sigma}_{r_k} < \texttt{tol}$, the step is accepted. Since this indicates that a sufficiently accurate approximation is available with a smaller rank, we determine the rank for the next step by
$$r_{k+1} = \max\left\{\operatorname{argmin}\{j \mid \widehat{\sigma}_{j+1} < \texttt{tol}\}, r_k - 2\right\},$$
i.e., the rank is reduced by either 1 or 2. This causes the rank to decay slowly and prevents sudden rank-drops. For the initial values in the next time step we use
$$\widetilde{S} = \widetilde{I}^T \Sigma_{k+1} \widetilde{I}, \qquad \widetilde{U} = (\widehat{U}_{k+1} P_{k+1})\widetilde{I}, \qquad \widetilde{V} = (\widehat{V}_{k+1} Q_{k+1})\widetilde{I},$$
where $\widetilde{I} = \begin{bmatrix} I_{r_{k+1}+1} \\ 0 \end{bmatrix} \in \mathbb{C}^{(r_k+1)\times(r_{k+1}+1)}$. To prevent rank-oscillations, rank reduction is prohibited within the first 10 steps after an augmentation step.
3. *Persistent case:* If $\widehat{\sigma}_{r_k} \geq \texttt{tol} > \widehat{\sigma}_{r_k+1}$, the time step is accepted and the same rank $r_{k+1} = r_k$ is used for the next one.

Just recently, the same idea for augmentation and reduction was used in [11].

3.2 Choice of tolerance

It remains to find a suitable tolerance `tol`. In the error analysis [14] of the projector-splitting integrator, the global error of the scheme is a combination of a time-discretization error and a low-rank error contribution. A similar result was derived in the error analysis of the ST-LO scheme in [10, Section 4]. We aim to choose the rank such that the low-rank error does not exceed the time discretization error. If the time discretization error is large, the low-rank error is allowed to be large as well, and hence the approximation rank might be chosen small. If the time discretization error

Algorithm 3 Augmentation

```
1: function AUGMENTATION($\widehat{U},\widehat{S},\widehat{V},\Delta A,r,\texttt{tol}$)
2:     {input: factors $\widehat{U},\widehat{S},\widehat{V}$ of rank-$(r+1)$ approximation $\widehat{A}=\widehat{U}\widehat{S}\widehat{V}^H$ with $\widehat{U}\in\mathscr{V}_{m,r+1}$, $\widehat{V}\in\mathscr{V}_{n,r+1}$,
3:         $\widehat{S}\in\mathbb{C}^{(r+1)\times(r+1)}$, functions for products with $\Delta A$, tolerance tol}
4:
5:     ready = False
6:     while not ready do
7:         $r=r+1$
8:         choose $u\in\mathbb{C}^m$ orthonormal to $\widehat{U}$ (e.g. random)
9:         choose $v\in\mathbb{C}^n$ orthonormal to $\widehat{V}$ (e.g. random)
10:        compute $\widehat{U}=U^*$, $S=S^*$, $V=V^*$ as in (15)
11:        $\widehat{U},\widehat{S},\widehat{V}=\mathrm{PRSI}(\widehat{U},\widehat{S},\widehat{V},r+1,\Delta A)$
12:        compute singular values $\widehat{\sigma}_1,\ldots,\widehat{\sigma}_{r+1}$ of $\widehat{S}$
13:        ready = $(\widehat{\sigma}_{r+1}<\texttt{tol})$
14:    end while
15:    return $\widehat{U},\widehat{S},\widehat{V},r$
16:    {output: factors $\widehat{U},\widehat{S},\widehat{V}$ of rank-$(r+1)$ approximation to $\widehat{A}+\Delta A$ with $\widehat{U}\in\mathscr{V}_{m,r+1}$, $\widehat{V}\in\mathscr{V}_{n,r+1}$,
17:        $\widehat{S}\in\mathbb{C}^{(r+1)\times(r+1)}$}
18: end function
```

is small, then the approximation rank needs to be sufficiently large to attain a small low-rank error.

The goal is to ensure that the rank-adaptivity does not impair the convergence order of the non-adaptive version of the low-rank integrator. To balance the low-rank error with the time discretization error, we use an estimator for the local error. The error analysis of the projector-splitting integrator given in [14] shows exponential growth of the error constant w.r.t. the final time T. For the ST-LO scheme, we also have shown such a behavior, cf. [10, Theorem 5]. However, numerical experiments indicate that this is a rather pessimistic bound. In practice, the error constants grow monotonically, but much slower in T for both the projector-splitting integrator and for the ST-LO scheme. For our implementation, we approximate the evolution of the error constants by piecewise linear functions. The respective slopes are recomputed every $M\in\mathbb{N}$ steps. Overall, the tolerance threshold `tol` is determined heuristically by the following steps:

1. Practical estimation of the local error: Starting from an approximation $\widehat{A}_{\ell M}\approx A(t_{\ell M})$, we compute an approximation to $A(t_{\ell M+1})$ with the rank-adaptive integrator by performing one step with step size τ. In this step, we prevent rank reduction. The rank of the (propagated) numerical approximation $\widehat{A}_{\ell M+1}$ is $r^*=r_{\ell M+1}+1$. The next time step is now performed with rank r^*, yielding the approximation $\widehat{A}_{\ell M+2}\approx A(t_{\ell M+2})$. Additionally, we perform four time steps with step size $\frac{\tau}{2}$ and rank r^*, starting from the initial value $\widehat{A}_{\ell M}$. By this, we obtain alternative approximations $\breve{A}_{\ell M+1}\approx A(t_{\ell M+1})$ and $\breve{A}_{\ell M+2}\approx A(t_{\ell M+2})$. Assuming that the method converges with order $p\in\mathbb{N}$ in time, we estimate the propagated errors of $\widehat{A}_{\ell M+1}$ and $\widehat{A}_{\ell M+2}$ by Richardson extrapolation [7, Section II.4] as

$$\|A(t_{\ell M+1})-\widehat{A}_{\ell M+1}\|\approx\frac{2^p}{2^p-1}\|\widehat{A}_{\ell M+1}-\breve{A}_{\ell M+1}\|=:\texttt{err}^{\mathrm{I}}_{\ell}.$$

and

$$\|A(t_{\ell M+2}) - \widehat{A}_{\ell M+2}\| \approx \frac{2^p}{2^p-1} \|\widehat{A}_{\ell M+2} - \breve{A}_{\ell M+2}\| =: \mathtt{err}_\ell^{\mathrm{II}},$$

cf. [8, Theorem 2.5]. We let

$$\zeta_\ell = \frac{\mathtt{err}_\ell^{\mathrm{II}}}{2\mathtt{err}_\ell^{\mathrm{I}}}$$

and assume that the propagated error of $\widehat{A}$ satisfies

$$\|A(t_{\ell M+j}) - \widehat{A}_{\ell M+j}\| \approx \mathtt{err}_\ell + j\zeta_\ell \mathtt{err}_\ell^{\mathrm{I}}, \qquad j = 1,2,\ldots,M, \tag{16}$$

where $\mathtt{err}_\ell$ is defined recursively via

$$\mathtt{err}_{\ell+1} = \mathtt{err}_\ell + M\zeta_\ell \mathtt{err}_\ell^{\mathrm{I}}, \qquad \ell = 0,1,\ldots, \qquad \mathtt{err}_0 = 0.$$

2. Estimation of the low-rank error: If $\sigma_1 \geq \ldots \geq \sigma_n \geq 0$ are the singular values of the exact solution $A(t_{k+1})$, then the rank-r_{k+1} best-approximation $\widehat{A}_{k+1}^{\text{best}}$ to $A(t_{k+1})$ fulfills

$$\frac{\|A(t_{k+1}) - \widehat{A}_{k+1}^{\text{best}}\|^2}{\|A(t_{k+1})\|^2} = \frac{\sigma_{r_{k+1}+1}^2 + \ldots + \sigma_n^2}{\sigma_1^2 + \ldots + \sigma_n^2} \leq \frac{(n - r_{k+1})\sigma_{r_{k+1}+1}^2}{\|\widehat{A}_{k+1}^{\text{best}}\|^2},$$

so that

$$\|A(t_{k+1}) - \widehat{A}_{k+1}^{\text{best}}\| \leq \sigma_{r_{k+1}+1} \frac{\|A(t_{k+1})\|}{\|\widehat{A}_{k+1}^{\text{best}}\|} \sqrt{n - r_{k+1}}. \tag{17}$$

3. The tolerance threshold $\mathtt{tol}_k$ is set by equating the right-hand sides of (16) and (17) for $k = \ell M + j$, where in (17) we replace the quotient of the unknown solution $A(t_{k+1})$ and its unknown best-approximation $\widehat{A}_{k+1}^{\text{best}}$ by 1, and the singular values σ_j by the numerically computed singular values $\widehat{\sigma}_j$. Solving

$$\widehat{\sigma}_{r_{k+1}+1} \sqrt{n - r_{k+1}} \overset{!}{\leq} \mathtt{err}_\ell + j\zeta_\ell \mathtt{err}_\ell^{\mathrm{I}}$$

for $\widehat{\sigma}_{r_{k+1}+1}$ yields the condition

$$\widehat{\sigma}_{r_{k+1}+1} \leq \frac{\mathtt{err}_\ell + j\zeta_\ell \mathtt{err}_\ell^{\mathrm{I}}}{\sqrt{n - r_{k+1}}} =: \mathtt{tol}_k. \tag{18}$$

These heuristics worked well in our numerical exeriments. However, they are only reliable if the time discretization error dominates the low-rank error. To ensure this, one must determine a suitable initial rank for the integration. One might use $r_0 = \text{rank}(A_0)$. However, if the rank of A_0 is very small, this may not necessarily hold for the rank of the exact solution $A(t)$ even for small times. On the other hand, if the rank of A_0 is large, this choice is also questionable. In our implementation, we first perform ν integration steps (with ν small, e.g. $\nu = 5$) with an initial rank given by the user (say $r_1 = 5$) and do not allow rank reduction in this phase. Then let r^* denote the number of singular values of $\widehat{A}_\nu$ greater or equal to $\mathtt{tol}_\nu$ defined in (18). If $r^* < r_1$, we continue the integration with $r_{\nu+1} = r^*$. Otherwise, we rerun the initializing process for rank r_1 multiplied by 2, until $r^* < r_1$ holds.

3.3 Rank-adaptive algorithms

The rank-adaptive version of the projector-splitting integrator Algorithm 1 is called RAPRSI for ***r**ank-**a**daptive **p**rojector-**s**plitting **i**ntegrator* in the following. A single step of the RAPRSI scheme is given in Algorithm 4.

Algorithm 4 Rank-adaptive projector-splitting integrator, single step

```
1: function RAPRSI($\widehat{U},\widehat{S},\widehat{V},r,\Delta A,\tau,p$)
2:     {input: factors $\widehat{U},\widehat{S},\widehat{V}$ of rank-$(r+1)$ approximation $\widehat{A}=\widehat{U}\widehat{S}\widehat{V}^H \approx A(t)$ with $\widehat{U}\in\mathcal{V}_{m,r+1}$,
3:             $\widehat{V}\in\mathcal{V}_{n,r+1}$, $\widehat{S}\in\mathbb{C}^{(r+1)\times(r+1)}$, functions for products with $\Delta A$, step size $\tau$}
4:
5:     $\widehat{U}_1,\widehat{S}_1,\widehat{V}_1 = $ PRSI$\big(\widehat{U},\widehat{S},\widehat{V},r+1,\Delta A\big)$
6:     compute SVD $\widehat{S}_1 = P\widehat{\sigma}Q^H$ where $\widehat{\sigma}=\mathrm{diag}(\widehat{\sigma}_1,\dots,\widehat{\sigma}_{r+1})$
7:     compute tol according to Section 3.2
8:     if $\widehat{\sigma}_r <$ tol then
9:         $r_1 = \mathrm{argmin}\{j \mid \widehat{\sigma}_{j+1} < \texttt{tol}\}$
10:        $\widetilde{I} = \big[I_{r_1+1}\ 0\big]^T \in \mathbb{C}^{(r+1)\times(r_1+1)}$
11:        $\widehat{U}_1 = (\widehat{U}_1 P)\widetilde{I}$
12:        $\widehat{S}_1 = \widetilde{I}^T\widehat{\sigma}\widetilde{I}$
13:        $\widehat{V}_1 = (\widehat{V}_1 Q)\widetilde{I}$
14:    else if $\widehat{\sigma}_{r+1} \geq$ tol then
15:        $\widehat{U}_1,\widehat{S}_1,\widehat{V}_1,r_1 = $ AUGMENTATION$(\widehat{U},\widehat{S},\widehat{V},\Delta A,r,\texttt{tol})$
16:    end if
17:    return $\widehat{U}_1,\widehat{S}_1,\widehat{V}_1,r_1$, optional $L=\widehat{V}_1\widehat{S}_1^H$
18:    {output: factors $\widehat{U}_1,\widehat{S}_1,\widehat{V}_1$ of rank-$(r_1+1)$ approximation $\widehat{A}_1=\widehat{U}_1\widehat{S}_1\widehat{V}_1^H \approx A(t+\tau)$ with
19:             $\widehat{U}_1\in\mathcal{V}_{m,r_1+1}$, $\widehat{V}_1\in\mathcal{V}_{n,r_1+1}$, $\widehat{S}_1\in\mathbb{C}^{(r_1+1)\times(r_1+1)}$}
20: end function
```

The rank-adaptive version of the ST-LO scheme is derived by replacing the PRSI routines by the RAPRSI routines. We name this new integrator ***r**ank-**a**daptive* **ST-LO** (RAST-LO) method. It is presented in Algorithm 5.

The rank-adaptive counterpart of the PRSISTIFF scheme is named RAPRSISTIFF. Since the linear subproblem preserves the rank, rank-adaptivity is only applied in the integration of the nonlinear subproblem (10b).

For stiff second-order matrix differential equations of the form (12), we equip the integrator ST-LOSTIFF with the adaptivity schemes described above. For the sake of efficiency, rank changes are only implemented in the integration of the nonlinear subproblem, even though the linear subproblems are in general not rank-preserving. Only in the case of rank augmentation in the integration of the nonlinear subproblem, the affected substeps of [10, Algorithm 3] are recomputed. This adaptive integrator is named RAST-LOSTIFF.

Algorithm 5 Rank-adaptive integrator for second-order ODEs, RASt-LO, full method

```
1: function RASt-LO($\tau, F, A_0, B_0$)
2:     {input: step size $\tau$, right-hand side $F$, initial values $A_0, B_0 \in \mathbb{C}^{m\times n}$}
3:
4:     compute initial ranks $r_A, r_B$ according to Section 3.2
5:     compute rank-$(r_A+1)$ best-approximation $\widehat{A} = \widehat{U}\widehat{S}\widehat{V}^H$, $\widehat{S} = \mathrm{diag}(\widehat{\sigma}_1, \dots, \widehat{\sigma}_{r_A}, \widehat{\sigma}_{r_A+1})$ to $A_0$
6:     compute rank-$(r_B+1)$ best-approximation $\widehat{B} = \widehat{T}\widehat{R}\widehat{W}^H$, $\widehat{R} = \mathrm{diag}(\rho_1, \dots, \rho_{r_B}, \rho_{r_B+1})$ to $B_0$
7:     $t_0 = 0$
8:     for $k = 1, \dots, n$ do
9:         $t_k = t_{k-1} + \tau$
10:
11:        $\widehat{B}$-step:
12:        $\widehat{T}, \widehat{R}, \widehat{W}, r_B, L = \mathrm{RAPRSI}\big(\widehat{T}, \widehat{R}, \widehat{W}, r_B, \Delta B, \tau, 2\big)$ where $\Delta B = \begin{cases} \frac{\tau}{2} F(\widehat{U}\widehat{S}\widehat{V}^H), & k = 1, \\ \tau F(\widehat{U}\widehat{S}\widehat{V}^H), & \text{else} \end{cases}$
13:
14:        $\widehat{A}$-step:
15:        $\widehat{U}, \widehat{S}, \widehat{V}, r_A = \mathrm{RAPRSI}\big(\widehat{U}, \widehat{S}, \widehat{V}, r_A, \Delta A, \tau, 2\big)$ where $\Delta A = \tau \widehat{T} L^H$
16:    end for
17:    $r = r_A$
18:    compute SVD $\widehat{S} = P\widehat{\sigma}Q^H$, $\widehat{U} = (UP)\widetilde{I}$, $\widehat{V} = (VQ)\widetilde{I}$, $\widehat{S} = \widetilde{I}^T\widehat{\sigma}\widetilde{I}$ where $\widetilde{I} = \big[I_r\ 0\big]^T \in \mathbb{C}^{(r+1)\times r}$
19:
20:    return $\widehat{U}, \widehat{S}, \widehat{V}$
21:    {output: factors $\widehat{U}, \widehat{S}, \widehat{V}$ of rank-$r$ approximation to exact solution $A(t_n)$ of (2) with $\widehat{U} \in \mathscr{V}_{m,r}$,
22:             $\widehat{V} \in \mathscr{V}_{n,r}$, $\widehat{S} \in \mathbb{C}^{r\times r}$}
23: end function
```

4 Numerical experiments

We conclude this paper with numerical experiments for matrix differential equations resulting from space discretizations of PDEs imposed on a rectangular domain

$$\Omega = [-L_x, L_x] \times [-L_y, L_y] \subset \mathbb{R}^2. \tag{19}$$

For simplicity, we use a uniform mesh with n grid points in x- and m grid points in y-direction, i.e.,

$$\begin{aligned} \Omega_h = \{(x_j, y_i) \mid x_j = -L_x + jh_x,\ y_i = -L_y + ih_y,\ 0 \le j \le n,\ 0 \le i \le m\}, \\ \text{with} \quad h_x = \frac{2L_x}{n}, \quad h_y = \frac{2L_y}{m}, \qquad n, m \in \mathbb{N}. \end{aligned} \tag{20}$$

Errors of the low-rank solutions are measured w.r.t. numerically computed reference solutions. Details are given in the respective subsections. Since we are only interested in the time discretization error, reference solutions and low-rank solutions are computed on the same spatial grid. The computation of the tolerance threshold as explained in Section 3.2 is performed with $M = 100$, i.e., every 100 steps we perform four additional steps with step size $\frac{\tau}{2}$, so that we increase the computational effort by 4%. Of course, choosing a smaller M leads to smaller errors, which might be necessary in some experiments, for instance in our first one.

All algorithms have been implemented in Python and were performed on a computer with an Intel(R) Core(TM) i7-7820X @ 3.60GHz CPU and 128 GB RAM storage. The codes are available from [21].

4.1 Nonlinear fractional Ginzburg–Landau equation

The fractional Ginzburg–Landau equation describes a variety of physical phenomena, cf. [18, 19, 24]. Here, we consider the problem in two space dimensions [25] and with homogeneous Dirichlet boundary conditions. Discretization in space by the second-order fractional centered difference method [3] yields the stiff semilinear matrix differential equation

$$A'(t) = -D_x A(t) - A(t) D_y - (\kappa + \mathrm{i}\xi) A(t) \bullet \overline{A(t)} \bullet A(t) + \gamma A(t), \quad A(0) = A_0. \quad (21)$$

Here, D_x and D_y are symmetric Toeplitz matrices [16] with first columns

$$\frac{\nu + \mathrm{i}\eta}{h_x^\alpha} \left[g_1^\alpha, g_2^\alpha, \dots, g_{n-1}^\alpha\right]^T \quad \text{and} \quad \frac{\nu + \mathrm{i}\eta}{h_y^\beta} \left[g_1^\beta, g_2^\beta, \dots, g_{m-1}^\beta\right]^T,$$

respectively. Further, $\mathrm{i} = \sqrt{-1}$, $\nu, \kappa > 0$, $\eta, \xi, \gamma \in \mathbb{R}$, $1 < \alpha, \beta < 2$ denote given parameters, and

$$g_k^\mu = \frac{(-1)^{k-1}\Gamma(1+\mu)}{\Gamma(\mu/2 - k + 2)\Gamma(\mu/2 + k + 2)}, \qquad \mu \in \{\alpha, \beta\}, \quad k \in \mathbb{Z},$$

where $\Gamma(\cdot)$ denotes the Gamma-function.

In [25], (21) was solved with the linearized second-order backward differential scheme (LBDF2). A fixed-rank dynamical low-rank integrator for (21) was proposed in [27], based on considerations from [20]. We compute low-rank solutions of (21) with PRSISTIFF and RAPRSISTIFF. The solution to the linear subproblem of (21), which is of form (11), is computed with the Krylov subspace method proposed in [16].

In our first experiment, we use the same parameter values as in [27], namely $L_x = L_y = 10$, $m = n = 512$, $\nu = \eta = \kappa = \xi = \gamma = 1$, $T = 1$, $\alpha = 1.2$, $\beta = 1.9$, and the initial value

$$(A_0)_{ij} = 2\,\mathrm{sech}(x_j)\,\mathrm{sech}(y_i)\,\mathrm{e}^{3\mathrm{i}(x_j + y_i)}, \qquad i, j = 1, \dots, m.$$

The (full-rank) reference solution is computed with LBDF2 on the same spatial grid, with time step size $\tau = 10^{-4}$. Figure 1 shows the relative global errors

$$\mathrm{err} = \frac{\|A - \widehat{A}\|}{\|A\|}$$

between the reference solution A and the respective low-rank solutions $\widehat{A}$ at $t = T$ for different step sizes τ. Convergence order one is observed for the PRSISTIFF scheme. For large step sizes, the approximations computed with the RAPRSISTIFF method exhibit large errors . This is explained by the behavior of the singular values, cf. Figure 1 (right picture). The time-discretization error is overestimated in this experiment, so that the tolerance threshold becomes so large that the second largest singular value is discarded. The induced low-rank error is then of magnitude 10^{-1}. If the parameter M is reduced to 30, this unfortunate rank reduction vanishes. However, reducing M

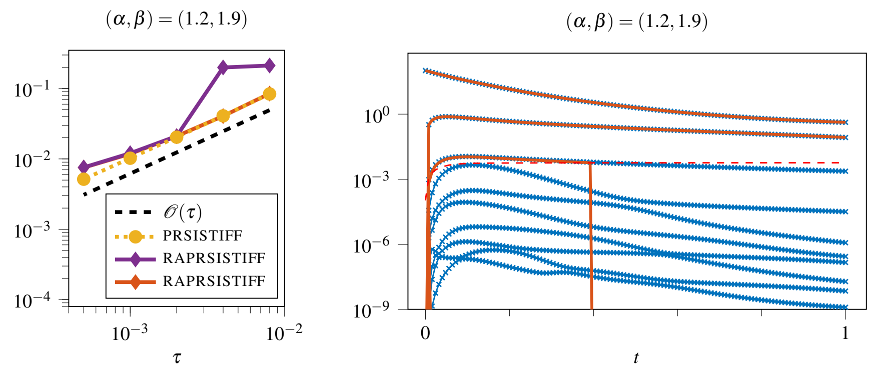

Fig. 1 Fractional Ginzburg–Landau equation, first experiment. The left picture shows the relative global error at $T = 1$ for $(\alpha,\beta) = (1.2,1.9)$, where the fixed-rank approximation (yellow) is computed with $r = 5$. The rank-adaptive approximation was computed with $M = 100$ (purple) and $M = 30$ (orange). The trajectories of the ten largest singular values of the reference solution (blue), the singular values of RAPRSISTIFF ($M = 30$) for $\tau = 1\cdot 10^{-3}$ (orange), and the computed tolerance threshold (red, dashed) are displayed on the right.

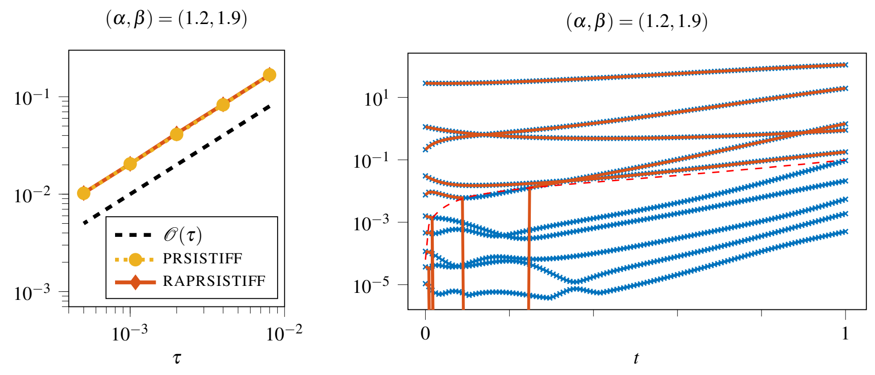

Fig. 2 Fractional Ginzburg–Landau equation, second experiment. The left picture shows the relative global error at $T = 1$ for $(\alpha,\beta) = (1.2,1.9)$, where the fixed-rank approximation is computed with $r = 8$. The trajectories of the ten largest singular values of the reference solution (blue), the singular values of RAPRSISTIFF for $\tau = 10^{-3}$ (orange), and the computed tolerance threshold (red, dashed) are displayed on the right.

increases the workload for the updates of `tol`, while $M = 100$ worked well in all other experiments and also in this experiment for smaller step sizes.

For our second example, we choose the second parameter set from [27], $L_x = L_y = 8$, $n = m = 512$, $\nu = \kappa = 1$, $\eta = 0.5$, $\xi = -5$, $\gamma = 3$, $\alpha = 1.2$, $\beta = 1.9$, and the initial values

$$(A_0)_{ij} = \mathrm{e}^{-2(x_j^2+y_i^2)}\,\mathrm{e}^{\mathrm{i}(S_0)_{ij}}, \qquad \text{where} \quad (S_0)_{ij} = (\mathrm{e}^{x_j+y_i} + \mathrm{e}^{-(x_j+y_i)})^{-1},$$

for $i = 1,\dots,m-1$, $j = 1,\dots,n-1$. The relative global errors at $T = 1$ are displayed in Figure 2. In contrast to the previous experiment, order one is observed for both integrators. Now the error curves for the fixed-rank integrator and its rank-adaptive

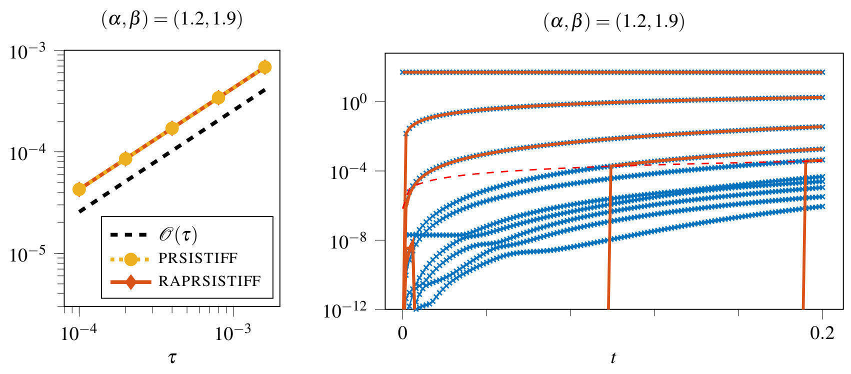

Fig. 3 Fractional Schrödinger equation. The left picture shows the relative global error at $T = 0.2$ for $(\alpha,\beta) = (1.2, 1.9)$, where the fixed-rank approximation is computed with $r = 5$. The trajectories of the ten largest singular values of the reference solution (blue), the singular values of RAPRSISTIFF ($M = 100$) for $\tau = 4 \cdot 10^{-4}$ (orange), and the computed tolerance threshold (red, dashed) are displayed on the right.

variant align almost perfectly, and the singular values follow nicely the trajectories of the singular values of the reference solution.

Similar results for both experiments were obtained for the parameter values $(\alpha,\beta) = (1.5, 1.5)$, $(1.7, 1.3)$, and $(1.9, 1.2)$, cf. [21].

4.2 Nonlinear fractional Schrödinger equation

The nonlinear fractional Schrödinger equation [26] is a special case of the fractional Ginzburg–Landau equation (21) with $\nu = \kappa = \gamma = 0$. For the limit $\alpha, \beta \to 2$ it becomes the classical Schrödinger equation.

In our experiment, the reference solution to the problem was again computed with the LBDF2 method, using the step size $\tau = 2 \cdot 10^{-5}$. Figure 3 shows the results for the parameter values from [26], $L_x = L_y = 10$, $n = m = 512$, $\eta = 1$, $\xi = -2$, $T = 0.2$, $\alpha = 1.2$, $\beta = 1.9$, and the initial value

$$(A_0)_{ij} = \operatorname{sech}(x_j)\operatorname{sech}(y_i)\exp(\mathrm{i}(x_j + y_i)), \qquad i, j = 1, \dots, m-1.$$

Again, the relative global error curves match almost perfectly for both low-rank methods, and are also clearly indicating convergence of order one. The results for other choices of α and β are available in [21].

4.3 Laser-plasma interaction

As an example for second-order problems, we consider a reduced model of laser-plasma interaction from [12, 13, 22]. It is given by a wave equation with space-dependent cubic nonlinearity on a bounded, rectangular domain Ω given in (19) with periodic boundary conditions. After space discretization according to [22, Section 4.1.3], we obtain the matrix differential equation

$$A''(t) = \mathscr{L}A(t) - 0.3\widetilde{\chi} \bullet \big(A(t) - \frac{1}{2}A(t) \bullet \overline{A(t)} \bullet A(t)\big) = F\big(A(t)\big), \tag{22}$$

with initial values $A(0) = A_0$ and $A'(0) = B_0$ given by

$$(A_0)_{ij} = 0.12 \exp\Big(-\frac{y_i^2}{l_0^2} - \frac{x_j^2}{w_0^2} + \mathrm{i}y_i\Big), \qquad (B_0)_{ij} = \Big(-\frac{2y_i}{l_0^2} - \mathrm{i}\Big)(A_0)_{ij},$$

where x_j, y_i are defined in (20) and $i = 1,\dots,m,\ j = 1,\dots,n$. The discrete Laplacian $\mathscr{L}$ acts on $A(t)$ via

$$\mathscr{L}A(t) = \mathscr{F}_m^{-1} D_y^2 \mathscr{F}_m A(t) + A(t)D_x,$$

where $D_x \in \mathbb{R}^{n\times n}$ denotes the symmetric Toeplitz matrix with first row

$$-\frac{1}{12h_x^2}\,[30, -16, 1, 0, \dots, 0, 1, -16]\,,$$

and

$$D_y = \frac{\mathrm{i}\pi}{L_y}\,\mathrm{diag}\Big(0, \dots, \frac{m}{2} - 1, -\frac{m}{2}, \dots, -1\Big)\,.$$

$\mathscr{F}_m$ denotes the discrete Fourier transformation operator for m Fourier modes and $\mathscr{F}_m^{-1}$ its inverse. Hence we use fourth order finite differences with n equidistant grid points in transversal direction and a pseudospectral method with m equidistant grid points in longitudinal direction.

Equation (22) describes the propagation of a laser pulse with wavelength λ_0 in the direction of the positive y-axis through vacuum and through a strongly localized plasma barrier. The plasma is located between $y = 50\pi$ and $y = 300\pi$ and has constant density 0.3. The localization is modeled by the matrix $\widetilde{\chi} \in \mathbb{R}^{m\times n}$ with entries

$$\widetilde{\chi}_{ij} = \begin{cases} 1, & 50\pi \le y_i \le 300\pi, \\ 0, & \text{else.} \end{cases} \tag{23}$$

The interaction between the pulse and the plasma is modeled by a cubic nonlinearity. As in [13] we use the parameters $\lambda_0 = \pi$, $l_0 = 10\pi$, $w_0 = 100\pi$, $L_x = 300\pi$, and $L_y = 600\pi$.

An efficient implementation of products $F(\widehat{A})E$ of the right-hand side $F(A)$ in (22) with a skinny matrix E is crucial. For the linear part, this is achieved by computing the matrix products in

$$(\mathscr{L}\widehat{A})E = \mathscr{F}_m^{-1} D_y^2 \mathscr{F}_m USV^H E + USV^H D_x E$$

successively from the right to the left. The implementation of the cubic nonlinear part of F is more involved and presented in detail in Appendix A.2.

Our numerical experiments were carried out for $t \in [0, 600\pi]$ with $n = 1024$ and $m = 8192$ discretization points in transversal and longitudinal direction, respectively. The reference solution was computed with the Gautschi-type method from [22], with

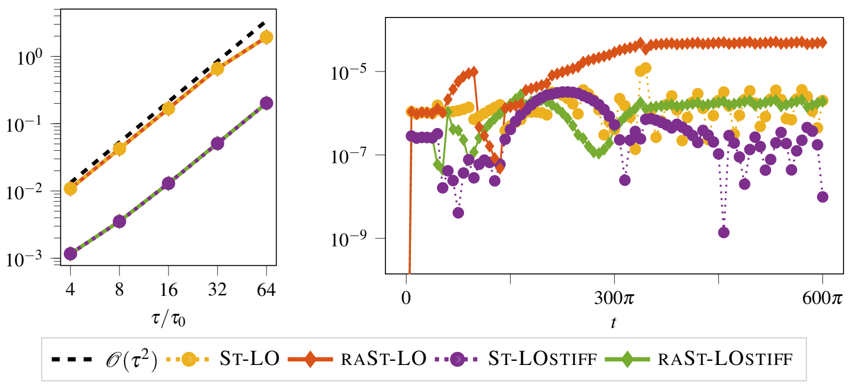

Fig. 4 Laser-plasma interaction. Relative global error between reference solution and low-rank approximations at $T = 600\pi$ (left), and absolute error in the maximal intensity for $\tau = 4\tau_0 = L_y/(20m)$ (right). The fixed-rank methods were computed with $r_A = r_B = 4$, the rank-adaptive methods with $M = 100$.

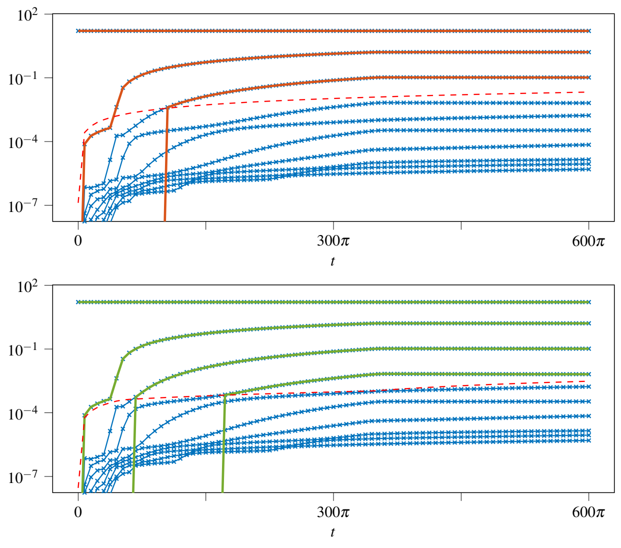

Fig. 5 Laser-plasma interaction. Trajectories of the ten largest singular values of the reference solution (blue) together with the trajectories of the singular values of the rank-adaptive low-rank integrators for $\tau = 4\tau_0$ (above: raSt-LO, below: raSt-LOstiff), and the respective computed tolerance thresholds (red, dashed).

step size $\tau_0 = L_y/(80m)$. For the low-rank solutions we used the step sizes $\tau = 2^k\tau_0$, $k = 2,\dots,6$. The algorithms St-LO and St-LOstiff were performed with fixed ranks $r_A = r_B = 4$. In the stiff methods St-LOstiff and raSt-LOstiff, we used the weights

$$\omega_1^2 = \frac{2}{3}, \quad \omega_2^2 = 0, \quad \omega_3^2 = \frac{1}{3}$$

in (13). This choice is motivated by the fact that the laser pulse moves mainly in longitudinal direction.

The left picture in Figure 4 shows the relative global error at $T = 600\pi$ between the reference solution and the different low-rank integrators. Second-order convergence is observed in all cases, and the stiff integrators yield better approximations than the nonstiff versions. The accuracy of the rank-adaptive schemes is comparable to those of the fixed-rank integrators, showing nicely that the heuristics works well for this example, cf. Figure 5.

In physics, the maximal intensity $\max_{i,j} |A_{ij}(t)|^2$ of the propagating pulse over time is sometimes of higher interest than A itself. In the right picture of Figure 4, the absolute error between the maximal intensity of the numerical pulse computed with the Gautschi-type integrator and the maximal intensity of the approximations obtained by the low-rank integrators is displayed.

4.4 Sine-Gordon equation

In our last experiment, we consider the two-dimensional sine-Gordon equation on the domain Ω from (19) with homogeneous Neumann boundary conditions [1]. Using finite differences of second order on the grid (20) with $L_x = L_y = 7$, $n = m = 1001$ in both x- and y-direction, we obtain the semi-discretized matrix differential equation

$$A''(t) = DA(t) + A(t)D^T - \Phi \bullet \underline{\sin}\left(A(t)\right), \quad t \in [0,T], \quad A \in \mathbb{C}^{(m+1)\times(m+1)}.$$

Here, $\underline{\sin}(A)$ denotes the entrywise evaluation of the sine function. The matrix D is given by

$$D = \frac{1}{h^2}\begin{pmatrix} -2 & 2 & & & \\ 1 & -2 & 1 & & \\ & \ddots & \ddots & \ddots & \\ & & 1 & -2 & 1 \\ & & & 2 & -2 \end{pmatrix} \in \mathbb{R}^{(m+1)\times(m+1)}, \qquad h = \frac{1}{m+1}.$$

The storage-economical evaluation of the products $\underline{\sin}(\widehat{A})E$ and $\underline{\sin}(\widehat{A})^H E$ is presented in Appendix A. There is no preferred direction of propagation, so that we used the weights

$$\omega_1^2 = \omega_2^2 = \omega_3^2 = \frac{1}{3}$$

in (13) for the ST-LOSTIFF and RAST-LOSTIFF methods .

First we consider the initial values

$$(A_0)_{ij} = 4\arctan\exp\left(\frac{x_j - 3.5}{0.954}\right), \qquad (B_0)_{ij} = 0.629\,\mathrm{sech}\left(\frac{x_j - 3.5}{0.954}\right),$$

and

$$\Phi_{ij} = 1 + \mathrm{sech}^2\sqrt{x_j^2 + y_i^2},$$

$i, j = 0, \ldots, m$, of a line soliton in an inhomogeneous medium [2, Section 3.1.3]. The reference solution is computed by the leapfrog scheme on the same spatial grid

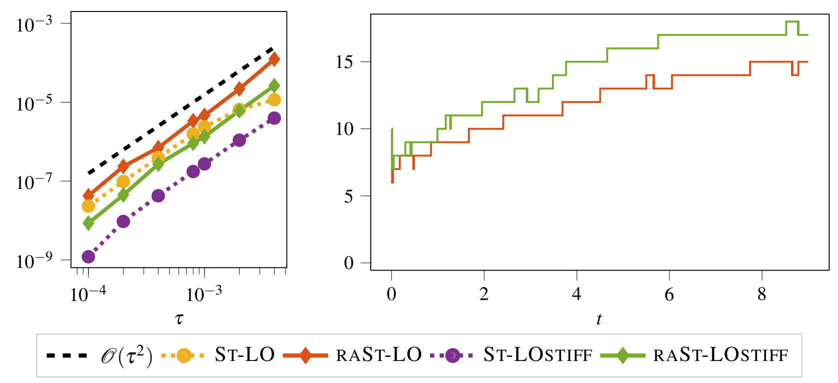

Fig. 6 Sine-Gordon equation, first setting. Relative global error at $T = 9$ between reference solution and low-rank approximations (left), and rank evolution of the solutions computed with the rank-adaptive integrators over time (right) for $\tau = 10^{-4}$. For the fixed-rank integrators, we used $r_A = r_B = 20$, for the rank-adaptive methods $M = 100$.

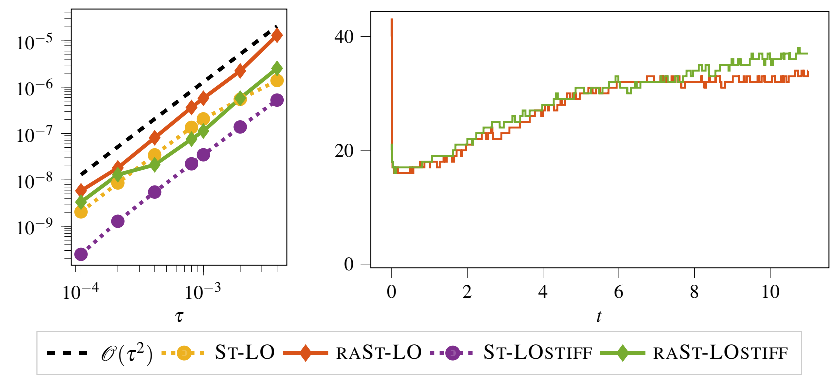

Fig. 7 Sine-Gordon equation, second setting. Relative global error at $T = 11$ between reference solution and low-rank approximations (left), and rank evolution of the solutions computed with the rank-adaptive integrators over time (right) for $\tau = 10^{-4}$. For the fixed-rank integrators, we used $r_A = r_B = 50$, for the rank-adaptive methods $M = 100$.

with time step size $\tau = 2.5 \cdot 10^{-5}$. Figure 6 shows the relative global errors between the low-rank approximations and the reference solution. Convergence order two is observed for all methods. The fixed-rank integrators are slightly more accurate than their rank-adaptive pendants, probably because they use a higher rank.

In a second setting, we consider the symmetric perturbation of a static line soliton [2, Section 3.1.2] with $\Phi_{ij} = 1$, $(B_0)_{ij} = 0$, and

$$(A_0)_{ij} = 4 \arctan \exp\left(x_j + 1 - \frac{2}{\cosh(y_i + 7)} - \frac{2}{\cosh(y_i - 7)}\right), \qquad i, j = 0, \dots, m.$$

Figure 7 shows a similar behavior of the methods as in the first setting. For the RAST-LO scheme however, the initial rank is rather large, and drops significantly after a few steps. This is caused in the routine for determining an appropriate initial rank. As explained in Section 3.2, the initial guess $r_1 = 5$ is doubled repeatedly until the criterion for continuing the integration beyond the first ν steps is satisfied. In this experiment, an initial rank of ~ 23 is adequate. Therefore, the guesses 5, 10, and 20 are rejected, until $r_1 = 40$ is accepted and rank reduction applies in the subsequent integration steps.

A Evaluation of entrywise functions for low-rank matrices

Let f be a (nonlinear) function that acts entrywise on matrices, let $E \in \mathbb{C}^{n\times r}$ be an arbitrary matrix, and let $\widehat{A} = \widehat{U}\widehat{S}\widehat{V}^H \in \mathscr{M}_r$ be a low-rank matrix with factors $\widehat{U}, \widehat{S}, \widehat{V}$ given in (5). For the efficiency of low-rank integrators for nonlinear problems, it is crucial to evaluate the product

$$f(\widehat{A})E, \tag{24}$$

using the factors $\widehat{U}$, $\widehat{S}$, and $\widehat{V}$ instead of the full matrix $\widehat{A}$. However, the entrywise computation of all components $\widehat{A}_{ij}$ of $\widehat{A}$ can not be avoided in general. Nevertheless, it is not necessary to store the full matrix $\widehat{A} \in \mathbb{C}^{m\times n}$, but it suffices to compute the rows of $\widehat{A}$ successively.

A.1 General functions

The ith row of $\widehat{A}$ is given by

$$(e_i\widehat{A}) = (e_i\widetilde{U})\widehat{V}^H \in \mathbb{C}^{1\times n}, \qquad i = 1,\dots,m,$$

where $\widetilde{U} = \widehat{U}\widehat{S}$. The matrix products $(e_i\widetilde{U})\widehat{V}^H$ are carried out with complexity $\mathscr{O}(nr)$. We now evaluate f entrywise at $e_i\widehat{A}$ and multiply the result with E, which gives the ith row of the product (24). This sequence of operations can be performed for each $i = 1,\dots,m$ independently and thus in parallel. This allows a fast computation, even for large m. Similarly, the evaluation of

$$C = f(\widehat{A})^H E, \qquad E \in \mathbb{C}^{m\times r},$$

is realized by computing the jth row via

$$(e_jC) = f(\widetilde{U}(e_j\widehat{V})^H)^H E, \qquad j = 1,\dots,n.$$

While this approach is suitable for any function f acting entrywise on its argument, e.g. trigonometric functions, the successive computation of the entries of $\widehat{A}$ can be avoided for monomials.

A.2 Monomials

Consider a (complex) monomial of degree $p \in \mathbb{N}$, $f(z) = z^p$ for $z \in \mathbb{C}$. The entrywise evaluation of f at $\widehat{A} \in \mathscr{M}_r$ is defined as $\big(f(\widehat{A})\big)_{ij} = \widehat{A}_{ij}^p$.

We now show how to compute the product (24) without computing or storing the elements of $\widehat{A}$ explicitly. Let $\widetilde{U} = \widehat{U}\widehat{S} \in \mathbb{C}^{m\times r}$. Then we have

$$\widehat{A} = \widehat{U}\widehat{S}\widehat{V}^H = \widetilde{U}\widehat{V}^H = \sum_{j=1}^{r} \widetilde{U}_j\widehat{V}_j^H, \tag{25}$$

where $\widetilde{U}_j$ is the jth column of $\widetilde{U}$ and $\widehat{V}_j$ the jth column of $\widehat{V}$, respectively. The Hadamard product is distributive and satisfies

$$(\widetilde{U}_j\widehat{V}_j^H) \bullet (\widetilde{U}_k\widehat{V}_k^H) = (\widetilde{U}_j \bullet \widetilde{U}_k)(\widehat{V}_j \bullet \widehat{V}_k)^H$$

for $1 \le j,k \le r$, cf. [23, Section 2]. Hence, for $E \in \mathbb{C}^{n\times r}$ it holds

$$\begin{aligned} f(\widehat{A})E &= \Bigg(\Big(\sum_{j_1=1}^{r} \widetilde{U}_{j_1} \widehat{V}_{j_1}^H \Big) \bullet \ldots \bullet \Big(\sum_{j_p=1}^{r} \widetilde{U}_{j_p} \widehat{V}_{j_p}^H \Big) \Bigg) E \\ &= \Bigg(\sum_{j_1,\ldots,j_p=1}^{r} \big(\widetilde{U}_{j_1} \bullet \widetilde{U}_{j_2} \bullet \ldots \bullet \widetilde{U}_{j_p} \big) \big(\widehat{V}_{j_1} \bullet \widehat{V}_{j_2} \bullet \ldots \bullet \widehat{V}_{j_p} \big)^H \Bigg) E \\ &= \sum_{j_1,\ldots,j_p=1}^{r} \big(\widetilde{U}_{j_1} \bullet \widetilde{U}_{j_2} \bullet \ldots \bullet \widetilde{U}_{j_p} \big) \big((\widehat{V}_{j_1} \bullet \widehat{V}_{j_2} \bullet \ldots \bullet \widehat{V}_{j_p})^H E \big). \end{aligned} \tag{26}$$

For the special case of the cubic nonlinearity which appears in the examples in Section 4.1, Section 4.2, and Section 4.3,

$$f(\widehat{A}) = \widehat{A} \bullet \overline{\widehat{A}} \bullet \widehat{A},$$

where $\overline{\widehat{A}}$ denotes the complex conjugate of $\widehat{A}$, (26) reads

$$(\widehat{A} \bullet \overline{\widehat{A}} \bullet \widehat{A})E = \sum_{j,k,\ell=1}^{r} \widetilde{U}_{jk\ell} \widehat{V}_{jk\ell}^H E, \qquad \text{where} \quad \widetilde{U}_{jk\ell} = \widetilde{U}_j \bullet \overline{\widetilde{U}}_k \bullet \widetilde{U}_\ell, \qquad \widehat{V}_{jk\ell} = \widehat{V}_j \bullet \overline{\widehat{V}}_k \bullet \widehat{V}_\ell.$$

The computational cost is further reduced by exploiting the symmetry in j and ℓ,

$$(\widehat{A} \bullet \overline{\widehat{A}} \bullet \widehat{A})E = \sum_{k=1}^{r} \Bigg[\sum_{j=1}^{r} \big(\widetilde{U}_j^2 \bullet \overline{\widetilde{U}}_k \big) \Big(\big(\widehat{V}_j^2 \bullet \overline{\widehat{V}}_k \big)^H E \Big) + 2 \sum_{j=1}^{r} \sum_{\ell=1}^{j-1} \widetilde{U}_{jk\ell} (\widehat{V}_{jk\ell}^H E) \Bigg]. \tag{27}$$

The product $(\widehat{A} \bullet \overline{\widehat{A}} \bullet \widehat{A})^H E$ with $E \in \mathbb{C}^{m\times r}$ can be computed analogously.

Additional simplifications apply to the product $(\widetilde{\chi} \bullet \widehat{A} \bullet \overline{\widehat{A}} \bullet \widehat{A})E$ with $\widetilde{\chi} \in \mathbb{C}^{m\times n}$ given in (23). It satisfies

$$\widetilde{\chi} = \begin{bmatrix} 0_{(\eta-1)\times n} \\ \mathbb{1}_{(\xi-\eta+1)\times n} \\ 0_{(m-\xi)\times n} \end{bmatrix} = \begin{pmatrix} 0_{\eta-1} \\ \mathbb{1}_{\xi-\eta+1} \\ 0_{m-\xi} \end{pmatrix} \mathbb{1}_n^T =: \widetilde{\mathbb{1}}_m \mathbb{1}_n^T, \tag{28}$$

where 0_n, $\mathbb{1}_n$ are the vectors of length n filled with zeros and ones, respectively, and $0_{n\times p}$ and $\mathbb{1}_{n\times p}$ the matrices of dimension $n \times p$ with all entries being zeros and ones, respectively. From (25) and (28), we obtain

$$\begin{aligned} (\widetilde{\chi} \bullet \widehat{A})E &= \Big[(\widetilde{\mathbb{1}}_m \mathbb{1}_n^T) \bullet \widehat{A} \Big] E = \Big[\sum_{j=1}^{r} \operatorname{diag}(\widetilde{\mathbb{1}}_m) \widetilde{U}_j \widehat{V}_j^H \operatorname{diag}(\mathbb{1}_n) \Big] E \\ &= \sum_{j=1}^{r} \begin{pmatrix} 0_{\eta-1} \\ \vartheta(\widetilde{U}_j) \\ 0_{m-\xi} \end{pmatrix} (\widehat{V}_j^H E) = \begin{bmatrix} 0_{(\eta-1)\times r} \\ \sum_{j=1}^{r} \vartheta(\widetilde{U}_j)(\widehat{V}_j^H)E \\ 0_{(m-\xi)\times r} \end{bmatrix}, \end{aligned}$$

where $\vartheta(\widetilde{U}_j)$ denotes the restriction of $\widetilde{U}_j$ to its ηth to ξth entries. Here, we made use of the following property of the Hadarmard product, cf. [23, Section 2]: If $A \in \mathbb{C}^{m\times n}$, $x \in \mathbb{R}^m$, and $y \in \mathbb{R}^n$, then

$$(xy^T) \bullet A = \operatorname{diag}(x) A \operatorname{diag}(y).$$

Hence, it suffices to compute the small matrices $\vartheta(\widetilde{U}_j)(\widehat{V}_j^H E)$ and sum them up. Likewise, using (27), we have

$$(\widetilde{\chi} \bullet \widehat{A} \bullet \overline{\widehat{A}} \bullet \widehat{A})E = \begin{bmatrix} 0_{(\eta-1)\times r} \\ \sum_{k=1}^{r} \Big[\sum_{j=1}^{r} \big(\vartheta(\widetilde{U}_j)^2 \bullet \vartheta(\overline{\widetilde{U}}_k) \big) \Big(\big(\widehat{V}_j^2 \bullet \overline{\widehat{V}}_k \big)^H E \Big) + 2 \sum_{j=1}^{r} \sum_{\ell=1}^{j-1} \vartheta(\widetilde{U}_{jk\ell})(\widehat{V}_{jk\ell}^H E) \Big] \\ 0_{(m-\xi)\times r} \end{bmatrix}.$$

The implementation of $(\widetilde{\chi} \bullet \widehat{A} \bullet \overline{\widehat{A}} \bullet \widehat{A})^H E$, $E \in \mathbb{C}^{m\times r}$, is realized in the same manner.

Acknowledgements Funded by the Deutsche Forschungsgemeinschaft (DFG, German Research Foundation) – Project-ID 258734477 – SFB 1173.

References

1. Bratsos, A.G.: An explicit numerical scheme for the sine-Gordon equation in $2+1$ dimensions. Appl. Numer. Anal. Comput. Math. **2**(2), 189–211 (2005). URL https://doi.org/10.1002/anac.200410035
2. Bratsos, A.G.: The solution of the two-dimensional sine-Gordon equation using the method of lines. J. Comput. Appl. Math. **206**(1), 251–277 (2007). URL https://doi.org/10.1016/j.cam.2006.07.002
3. Çelik, C., Duman, M.: Crank-Nicolson method for the fractional diffusion equation with the Riesz fractional derivative. J. Comput. Phys. **231**(4), 1743–1750 (2012). URL https://doi.org/10.1016/j.jcp.2011.11.008
4. Ceruti, G., Kusch, J., Lubich, C.: A rank-adaptive robust integrator for dynamical low-rank approximation. CRC 1173 Preprint 2021/16, Karlsruhe Institute of Technology (2021). URL https://www.waves.kit.edu/downloads/CRC1173_Preprint_2021-16.pdf
5. Ceruti, G., Lubich, C.: An unconventional robust integrator for dynamical low-rank approximation. CRC 1173 Preprint 2020/41, Karlsruhe Institute of Technology (2020). URL https://www.waves.kit.edu/downloads/CRC1173_Preprint_2020-41.pdf. Accepted by BIT Numerical Mathematics
6. Dektor, A., Rodgers, A., Venturi, D.: Rank-adaptive tensor methods for high-dimensional nonlinear pdes (2021). URL https://arxiv.org/pdf/2012.05962.pdf
7. Hairer, E., Nørsett, S.P., Wanner, G.: Solving ordinary differential equations I: Nonstiff problems, *Springer Series in Computational Mathematics*, vol. 8, second edn. Springer-Verlag, Berlin (1993). URL https://doi.org/10.1007/978-3-540-78862-1
8. Henrici, P.: Discrete variable methods in ordinary differential equations. John Wiley & Sons, Inc., New York-London (1962)
9. Hesthaven, J., Pagliantini, C., Ripamonti, N.: Rank-adaptive structure-preserving reduced basis methods for Hamiltonian systems. – (2020). URL https://pure.tue.nl/ws/portalfiles/portal/169030473/2007.13153v1.pdf
10. Hochbruck, M., Neher, M., Schrammer, S.: Dynamical low-rank integrators for second-order matrix differential equations. CRC 1173 Preprint 2022/12, Karlsruhe Institute of Technology (2022). DOI 10.5445/IR/1000143003. URL https://www.waves.kit.edu/downloads/CRC1173_Preprint_2022-12.pdf
11. Hu, J., Wang, Y.: An adaptive dynamical low rank method for the nonlinear boltzmann equation (2021). URL https://arxiv.org/pdf/2112.02695.pdf
12. Karle, C., Schweitzer, J., Hochbruck, M., Laedke, E.W., Spatschek, K.H.: Numerical solution of nonlinear wave equations in stratified dispersive media. J. Comput. Phys. **216**(1), 138–152 (2006). URL https://doi.org/10.1016/j.jcp.2005.11.024
13. Karle, C., Schweitzer, J., Hochbruck, M., Spatschek, K.H.: A parallel implementation of a two-dimensional fluid laser-plasma integrator for stratified plasma-vacuum systems. J. Comput. Phys. **227**(16), 7701–7719 (2008). URL https://doi.org/10.1016/j.jcp.2008.04.024
14. Kieri, E., Lubich, C., Walach, H.: Discretized dynamical low-rank approximation in the presence of small singular values. SIAM J. Numer. Anal. **54**(2), 1020–1038 (2016). URL https://doi.org/10.1137/15M1026791
15. Koch, O., Lubich, C.: Dynamical low-rank approximation. SIAM J. Matrix Anal. Appl. **29**(2), 434–454 (2007). URL https://doi.org/10.1137/050639703
16. Lee, S.T., Pang, H.K., Sun, H.W.: Shift-invert Arnoldi approximation to the Toeplitz matrix exponential. SIAM J. Sci. Comput. **32**(2), 774–792 (2010). URL https://doi.org/10.1137/090758064
17. Lubich, C., Oseledets, I.V.: A projector-splitting integrator for dynamical low-rank approximation. BIT **54**(1), 171–188 (2014). URL https://doi.org/10.1007/s10543-013-0454-0
18. Milovanov, A., Rasmussen, J.J.: Fractional generalization of the Ginzburg–Landau equation: an unconventional approach to critical phenomena in complex media. Physics Letters A **337**(1), 75 – 80 (2005). URL https://doi.org/10.1016/j.physleta.2005.01.047
19. Mvogo, A., Tambue, A., Ben-Bolie, G.H., Kofané, T.C.: Localized numerical impulse solutions in diffuse neural networks modeled by the complex fractional Ginzburg-Landau equation. Commun. Nonlinear Sci. Numer. Simul. **39**, 396–410 (2016). URL https://doi.org/10.1016/j.cnsns.2016.03.008
20. Ostermann, A., Piazzola, C., Walach, H.: Convergence of a low-rank Lie-Trotter splitting for stiff matrix differential equations. SIAM J. Numer. Anal. **57**(4), 1947–1966 (2019). URL https://doi.org/10.1137/18M1177901

21. Schrammer, S.: Codes for numerical experiments (2022). URL https://doi.org/10.5445/IR/1000143199
22. Schweitzer, J.: Numerical Simulation of Relativistic Laser–Plasma Interaction. Phd thesis, Heinrich Heine University Düsseldorf (2008). URL https://docserv.uni-duesseldorf.de/servlets/DocumentServlet?id=8401
23. Styan, G.P.H.: Hadamard products and multivariate statistical analysis. Linear Algebra Appl. **6**, 217–240 (1973). URL https://doi.org/10.1016/0024-3795(73)90023-2
24. Tarasov, V.: Psi-series solution of fractional Ginzburg–Landau equation. Journal of Physics A **39**, 8395–8407 (2006)
25. Zhang, Q., Lin, X., Pan, K., Ren, Y.: Linearized ADI schemes for two-dimensional space-fractional nonlinear Ginzburg-Landau equation. Comput. Math. Appl. **80**(5), 1201–1220 (2020). URL https://doi.org/10.1016/j.camwa.2020.05.027
26. Zhao, X., Sun, Z.z., Hao, Z.p.: A fourth-order compact ADI scheme for two-dimensional nonlinear space fractional Schrödinger equation. SIAM J. Sci. Comput. **36**(6), A2865–A2886 (2014). URL https://doi.org/10.1137/140961560
27. Zhao, Y.L., Ostermann, A., Gu, X.M.: A low-rank Lie-Trotter splitting approach for nonlinear fractional complex Ginzburg-Landau equations (2020)